Temperature-stable $Y_{2.95}Dy_{0.05}MgAl_3SiO_{12}$ garnet-type 5G millimeter-wave dielectric ceramic resonator antenna

Yu Jiang[1], Huan Liu[1,*], Zhiyu Xiu[1], Guofa Wu[1], Minmin Mao[1,*], Xinjiang Luo[1], Bing Liu[1], Zhilun Lu[2], Zeming Qi[3], Dongyang Sun[2], Kaixin Song[1,*]

1. *College of Electronic Information, Hangzhou Dianzi University, Hangzhou, 310018, China*
2. *School of Engineering and the Built Environment, Edinburgh Napier University, Edinburgh EH10 5DT, UK*
3. *National Synchrotron Radiation Laboratory, University of Science and Technology of China, Hefei, 230029, P. R. China*

ABSTRACT

Temperature stability is a crucial property of microwave electronic components, as well as a pivotal aspect of assessing the performance of microwave dielectric ceramics. In this article, the temperature coefficient of high-$Q\times f$ garnet-type $Y_{2.95}Dy_{0.05}MgAl_3SiO_{12}$ microwave ceramic was regulated by doping with different mass ratios of TiO_2. Further, combined with the Kramers-Kronig (K-K) formula, the dielectric loss and theoretical permittivity of $Y_{2.95}Dy_{0.05}MgAl_3SiO_{12}$-9wt%$TiO_2$ ceramic are calculated by infrared reflection spectrum data, which coincide exactly with the experimental results. Importantly, a 5G millimeter-wave antenna was fabricated with $Y_{2.95}Dy_{0.05}MgAl_3SiO_{12}$-9wt%$TiO_2$ ceramic and tested at 25 ℃ and 85 ℃, respectively. The center frequencies of measurement are 25.99 GHz at 25 °C and 26.12 GHz at 85 °C, and the frequency shift with temperature is rather low, showing excellent temperature stability. The simulated efficiency of 88.5% and gain of 6.05 dBi also indicate that the antenna has favorable radiation characteristics. The results show that the temperature-stable $Y_{2.95}Dy_{0.05}MgAl_3SiO_{12}$-9wt%$TiO_2$ ceramic antenna has broad prospect in 5G millimeter wave communication.

Keywords: Infrared reflectivity spectroscopy; Garnet; Millimeter-wave antenna

1. Introduction

* Corresponding Authors: liuhuan9430@163.com; mmm@hdu.edu.cn; kxsong@hdu.edu.cn;

As the amount of data in the network continues to increase, the communication system needs to improve the transmission speed and carrying capacity, and the frequency band trend of mobile communication is also moving towards the high frequency band [1-3]. The high-frequency band of 5G mobile communication is in the millimeter wave region [4]. In the future, 6G communication frequency will rise to the terahertz frequency band. The continuous increase in frequency also puts forward higher requirements for ceramic materials [5-7]. Ceramic materials are an indispensable part of electronic components. Compared to metal materials, ceramic materials have the stable temperature coefficient and ultra-low dielectric loss. These advantages are especially evident in high-frequency communication systems [8-10].

Ceramic materials are widely used in electronic components, such as dielectric substrates, dielectric resonators, ceramic filters, etc. [11-15]. J.F. Ziircher [16] designed and tested microstrip patch antennas for GPS systems using ceramic material and RT/Duroid 6010 dielectric substrate, respectively, over a temperature range of -5 to +44 °C. The results show that temperature has a large influence on the resonance frequency of the RT/Duroid 6010 antenna, and the applicable temperature range is narrow, ranging from 15 to 25 °C. While with a ceramic substrate, the antenna's center frequency changes very little with temperature (about 0.2%) and matches well across all thermal ranges. And for dielectric resonators, G. Drossos *et al.* [17] designed a cylindrical dielectric resonator antenna and examined its performance at different temperatures (300 K and 77 K). The resonance frequency and return loss of the DRA vary with temperature. It is noticeable that temperature stability must also be regulated in addition to enhance the $Q\times f$ value of microwave dielectric ceramics.

Garnet-typed microwave ceramics have attracted more attention owing to their low ε_r, high $Q\times f$ value and adjustable τ_f [18-21]. Furthermore, when compared to other low dielectric constant systems, garnet has a stable crystal structure, a wide range of synthesis stability, and a simple preparation process, all of which contribute to its high application potential [22-23]. The dielectric constant of garnet-type microwave dielectric ceramics is generally around 10, making them low-dielectric ceramics that are ideal for low-latency 5G high-frequency communication [24]. In addition to dielectric constant, ceramic materials used in electronic components must have a high $Q\times f$ and a near-zero τ_f [25-27]. Zhou *et al.* [28] reported a very high $Q\times f$ of 234,936

GHz by adding excess Y and sintering in a vacuum of 1750 °C for 12 hours, without adjusting the τ_f, and with a high sintering temperature and long sintering time.

The authors' group studied $Y_3MgAl_3SiO_{12}$ garnet-type ceramics, which successfully reduced the sintering temperature to 1550 °C and the sintering time to 4 hours, while exhibiting excellent microwave dielectric properties: ε_r = 10.1, $Q\times f$ = 57,340 GHz and τ_f = -32 ppm/°C [29]. Further, the $Q\times f$ was increased by ~20% via the strategy of Dy^{3+} substitution in the Y^{3+} lattice site for $Y_{2.95}Dy_{0.05}MgAl_3SiO_{12}$ microwave ceramic (ε_r = 9.68, $Q\times f$ = 68,866 GHz, τ_f = -38.5 ppm/°C). However, it still has a large negative value for its temperature coefficient, making its practical application challenging. In order to adjust τ_f of $Y_{2.95}Dy_{0.05}MgAl_3SiO_{12}$ ceramic to near zero, a material with a positive temperature coefficient, such as TiO_2 (τ_f~ +460 ppm/°C) was added as compensation [30-31]. (1-*x*)$Y_{2.95}Dy_{0.05}MgAl_3SiO_{12}$- *x*wt%$TiO_2$ (*x* = 0-9) microwave ceramics were therefore prepared, and the effects of various TiO_2 concentrations on bulk density, grain size and dielectric properties were studied. Moreover, a millimeter-wave antenna was fabricated based on temperature stable $Y_{2.95}Dy_{0.05}MgAl_3SiO_{12}$-9wt%$TiO_2$ ceramic and tested at 25 °C and 85 °C, respectively.

2. Experimental

2.1 Synthetic samples

(1-*x*)$Y_{2.95}Dy_{0.05}MgAl_3SiO_{12}$-*x* wt%$TiO_2$ (*x* = 0-9) ceramics were synthesized by solid-state reaction method. High-purity raw materials of Y_2O_3 (99.99%), Dy_2O_3 (99.99%), MgO (99.99%), Al_2O_3 (99.99%), SiO_2 (99.99%) were weighed on the basis of stoichiometric ratio and the obtained raw materials were ball-milled in solvent ethanol for 12 h. And the dried powders were calcined at 1575 °C for 4 h. The composite materials were ball milled in absolute ethanol for 12 h after adding different mass ratios of TiO_2. The mixed powders were calcined at 1300 °C for 4 hours. The calcined powders were reground and uniformly mixed with 5wt% PVA. The powders were pressed into cylindrical particles (thickness: 7-8mm, diameter: 12.7mm) and then sintered at 1450-1625 °C for 5 h.

2.2 Characterization

The phase compositions and crystal structure were identified by X-ray diffraction (Shimadzu, Kyoto, Japan) using Cu-Kα radiation with a scanning angle of 10-80° and a step size of 0.02°. The microstructure was observed by the scanning electron microscope (Sigma 300, ZEISS). The Archimedes method was used to determine the bulk density. Microwave dielectric properties were measured in $TE_{01\delta}$ mode using the resonant cavity method. The Keysight (N5234B) vector network analyzer was used for evaluating the $Q\times f$ values and ε_r as well as the return loss (S_{11}) measurement. The τ_f value was obtained by the following formula:

$$\tau_f = \frac{f_{85} - f_{25}}{f_{25} \times (85 - 25)} \tag{1}$$

where f_{25} and f_{85} denote the resonance frequencies at 25 °C and 85°C, respectively.

2.3 Antenna design and fabrication

The dielectric resonator antenna is simulated by HFSS, and the DRA size is related to $\frac{\lambda_0}{\sqrt{\varepsilon_r}}$, where λ_0 is the wavelength at resonant frequency and ε_r is the dielectric constant of the DR. Thus for the same frequency, a high dielectric constant can reduce the size of DR [32].

The design formulas of typical rectangular dielectric resonant antenna by means of numerical calculation and curve fitting are as follows [33-34]:

$$f_{GHz} = \frac{15F}{w_{cm}\pi\sqrt{\varepsilon_r}} \tag{2}$$

$$F = a_0 + a_1(\frac{w}{b}) + a_2(\frac{w}{b})^2 \tag{3}$$

$$a_0 = 2.57 - 0.8(\frac{d}{b}) + 0.42(\frac{d}{b})^2 - 0.05(\frac{d}{b})^3 \tag{4}$$

$$a_1 = 2.71(\frac{d}{b})^{-0.282} \tag{5}$$

$$a_2 = 0.16 \tag{6}$$

where w_{cm} is expressed in cm and the resonant frequency will be in GHz, $w \times d \times b/2$ is

the dimension of the DRA.

The following formulas can be used as a starting point for rectangular slots:

$$l_s = \frac{0.4\lambda_0}{\sqrt{\varepsilon_e}} \tag{7}$$

$$\varepsilon_e = \frac{\varepsilon_r + \varepsilon_s}{2} \tag{8}$$

$$w_s = 0.2 l_s \tag{9}$$

where l_s and w_s are the slot length and width, respectively, ε_r and ε_s are the dielectric constants of the DRA and substrate, respectively.

The stub extension s is selected so that its reactance cancels out that of the slot aperture. It is generally initially chosen to be:

$$s = \frac{\lambda_g}{4} \tag{10}$$

where λ_g is the guide wave in the substrate.

The proposed antenna consisted primarily of a dielectric substrate, a rectangular dielectric resonator fabricated by $Y_{2.95}Dy_{0.05}MgAl_3SiO_{12}$-9wt%$TiO_2$, and a SMA connector that was excited by aperture coupling and exhibited excellent radiation characters. The rectangular dielectric resonator of the antenna was obtained by grinding the cylindrical sample into a rectangle. And an adhesive tape on the grounding plate is used to fix the dielectric resonator. The Keysight (N5234B) supports a frequency range of 10 MHz to 43.5 GHz, and the SMA connector supports a frequency range of DC - 40 GHz. And the antenna was tested at different temperature (25 °C and 85 °C). The antenna was heated on a heating table, and the temperature of the antenna was measured using an infrared thermometer (-32 ℃~380 ℃) to ensure the temperature reached 85 °C.

3. Results and discussion

The bulk densities of (1-x)$Y_{2.95}Dy_{0.05}MgAl_3SiO_{12}$-$x$ wt%TiO_2 (x = 0-9) ceramics sintered at 1450 ℃-1625 ℃ are plotted in Fig. 1(a). The bulk densities of composite ceramics containing various mass fractions of TiO_2 increase markedly and then

decrease as sintering temperature rising. Furthermore, the maximum bulk density of (1-*x*)$Y_{2.95}Dy_{0.05}MgAl_3SiO_{12}$-*x* wt%$TiO_2$ (*x* = 0-9) ceramics gradually decreases from 4.46 g/cm^3 to 4.3 g/cm^3 as the TiO_2 mass fraction increases. This is because density of TiO_2 (4.23 g/cm^3) is lower than that of $Y_{2.95}Dy_{0.05}MgAl_3SiO_{12}$ (4.46 g/cm^3) [35]. The optimal sintering temperature decreases as the TiO_2 content increases, indicating that TiO_2 is beneficial in reducing the sintering temperature. Fig. 1 (b) shows the relative densities of TiO_2 doped with different mass fractions at the optimum sintering temperature. With the increase of TiO_2 doping content, the relative density decreases from 98.28% (*x*=0) to 94.55% (*x*=9), which is consistent with the change trend of $Q \times f$ value.

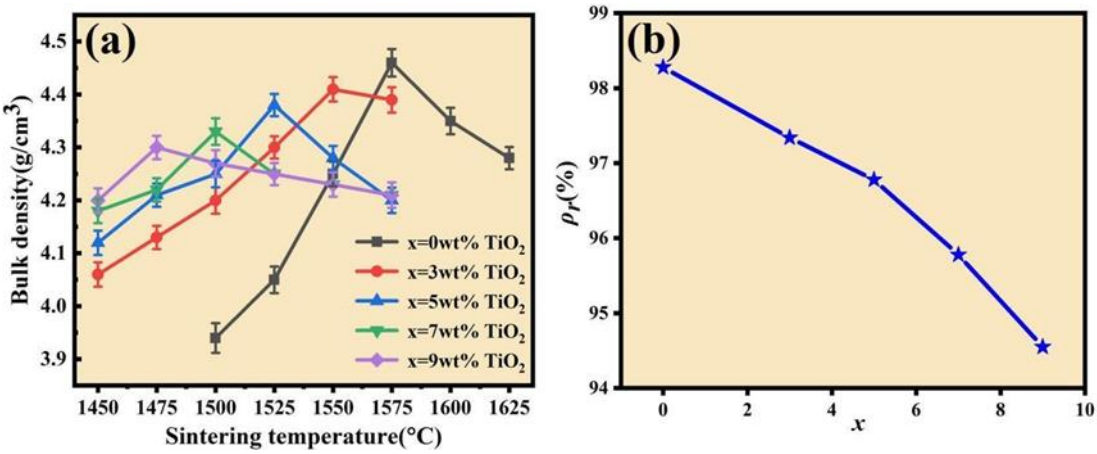

Fig. 1. The bulk densities of (1-*x*)$Y_{2.95}Dy_{0.05}MgAl_3SiO_{12}$-*x*wt%$TiO_2$ (*x*=0-9) composite ceramics varies with sintering temperature. (b) Relative densities of TiO_2 doped with different mass fractions at the optimum sintering temperature.

Fig. 2 illustrates the XRD patterns of (1-*x*)$Y_{2.95}Dy_{0.05}MgAl_3SiO_{12}$-*x* wt%$TiO_2$ (*x* = 0-9) ceramics at optimal sintering temperature. When TiO_2 is not added (*x*=0), all diffraction peaks are indexed to $Y_3Al_5O_{12}$ (PDF#82-0575) garnet. As the mass fraction of TiO_2 increases, the main diffraction peaks correspond to the $Y_3Al_5O_{12}$ phase, while the others correspond to two phases of TiO_2 (PDF#73-1764) and $Y_2Ti_2O_7$ (PDF#85-1570). The appearance of the $Y_2Ti_2O_7$ phase is due to the limited solid solubility of TiO_2 in $Y_{2.95}Dy_{0.05}MgAl_3SiO_{12}$. When *x* = 3, the phases of TiO_2 and $Y_2Ti_2O_7$ are not obvious, and a portion of TiO_2 may be solid-dissolved into $Y_{2.95}Dy_{0.05}MgAl_3SiO_{12}$ crystal. With increasing TiO_2 concentration, the phases of TiO_2 and $Y_2Ti_2O_7$ gradually become more stable. When the TiO_2 concentration exceeds the limiting value, the secondary phase $Y_2Ti_2O_7$ forms, as confirmed in the published literature [36-38].

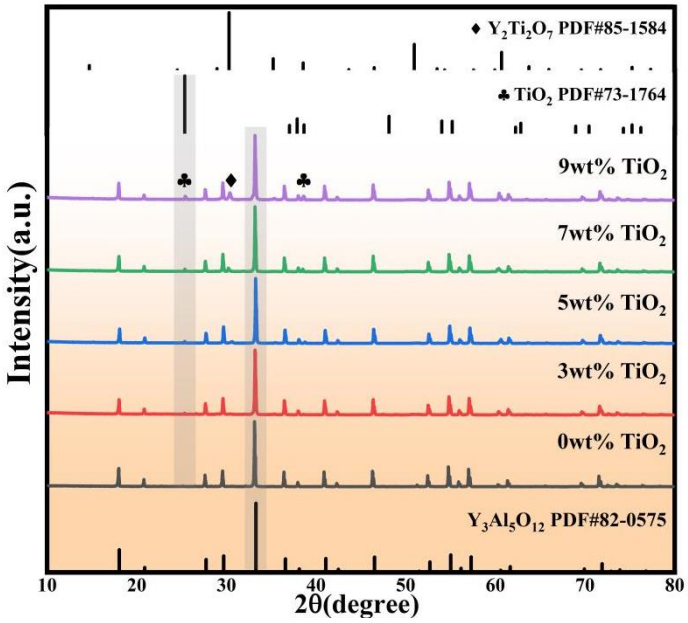

Fig. 2. XRD of (1-*x*)$Y_{2.95}Dy_{0.05}MgAl_3SiO_{12}$-*x* wt%$TiO_2$ (*x* = 0-9) ceramics.

The SEM micrographs of (1-*x*)$Y_{2.95}Dy_{0.05}MgAl_3SiO_{12}$-*x*wt%$TiO_2$(*x*=0-9) ceramics are demonstrated in Fig. 3(a-e). The average grain size and grain distribution of the composite ceramic samples, as measured by Image J software, are shown in the insets. From the SEM images of all samples (Fig. 3 (a-e)), the surface grain boundaries of the composite ceramic samples are relatively clear, the grain size distribution is uniform, and there are no obvious pores, indicating that all composite ceramics have relatively high densities. Fig. 3(f) shows the trend of the average grain size of composite ceramics varies with TiO_2 content. As the mass percentage of TiO_2 increases, the average grain size falls off from 6.12 μm (*x*=0) to 4.20 μm (*x*=9), indicating that the increase of TiO_2 content inhibits the growth of $Y_{2.95}Dy_{0.05}MgAl_3SiO_{12}$ ceramic grains.

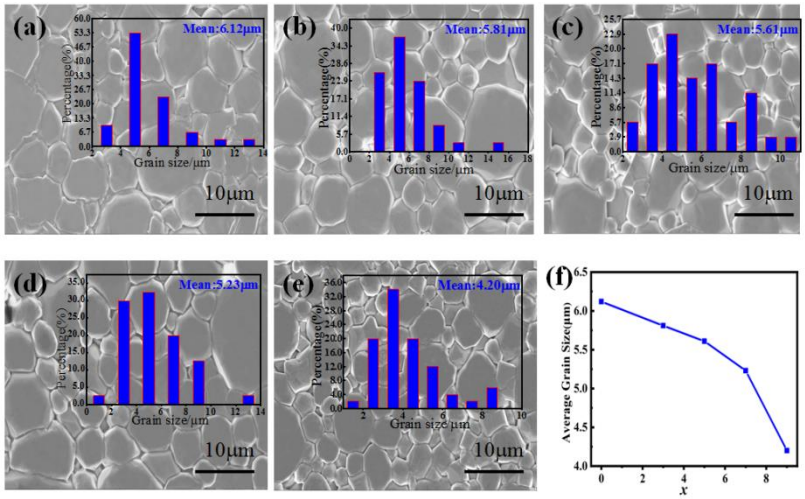

Fig. 3. SEM images of (1-*x*)$Y_{2.95}Dy_{0.05}MgAl_3SiO_{12}$-*x* wt%$TiO_2$ (*x*= 0-9) ceramics: (a) *x* = 0; (b) *x* = 3; (c) *x* = 5; (d) *x* = 7; (e) *x* = 9. (f) The average grain size of composite ceramics.

Fig. 4 plots the microwave dielectric properties of (1-*x*)$Y_{2.95}Dy_{0.05}MgAl_3SiO_{12}$-*x*wt%$TiO_2$ (*x* = 0-9) ceramics. The ε_r increases gradually from 9.68 (*x* = 0) to 12.06 (*x* = 9), as shown by the changing trend of the black curve in Fig. 4. This is because the TiO_2 (ε_r ~ 105) possesses a higher dielectric constant than $Y_{2.95}Dy_{0.05}MgAl_3SiO_{12}$ ceramic (ε_r ~ 9.68) [39]. The red curve represents the trend of change in the $Q\times f$ value of composite ceramics with various mass fractions of TiO_2. And the $Q\times f$ value drops sharply from 68,866 GHz to 28,604 GHz because the $Q\times f$ value of TiO_2 (~46,000 GHz) is lower than that of $Y_{2.95}Dy_{0.05}MgAl_3SiO_{12}$ (~68,866 GHz), and the addition of TiO_2 introduces the secondary phase $Y_2Ti_2O_7$, whose $Q\times f$ value is only 9,000 GHz, which is much smaller than TiO_2 (~ 46,000 GHz) and $Y_{2.95}Dy_{0.05}MgAl_3SiO_{12}$ (~68,866 GHz) [36,40]. In addition, the grain boundaries among $Y_{2.95}Dy_{0.05}MgAl_3$ SiO_{12}, TiO_2 and $Y_2Ti_2O_7$ increase as the mass fraction of TiO_2 increases, resulting in greater lattice distortion between different grain boundaries, which is also one of the reasons for the sharp decline in $Q\times f$ value. And the blue curve is the variation trend of the temperature coefficient (τ_f) of the composite ceramics. Since TiO_2 has a high positive temperature coefficient (τ_f ~ + 460 ppm/°C), increasing the mass fraction of TiO_2 improves the temperature coefficient of the composite ceramics effectively [41]. When *x* = 9, the temperature coefficient is close to zero and the specific τ_f value is -3.4ppm/°C.

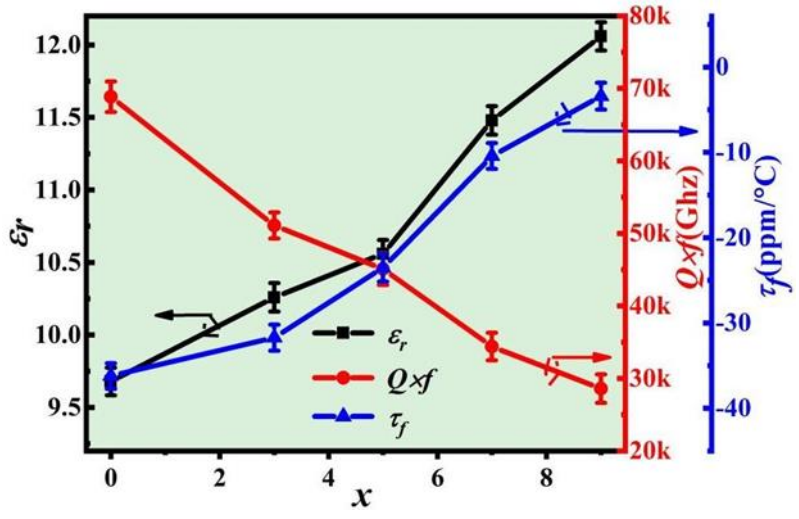

Fig. 4. Microwave dielectric properties of (1-*x*) $Y_{2.95}Dy_{0.05}MgAl_3SiO_{12}$-*x* wt%$TiO_2$ (*x*= 0-9) ceramics.

For purpose of further analyzing the association between the inherent microwave dielectric properties of $Y_{2.95}Dy_{0.05}MgAl_3SiO_{12}$-9wt%$TiO_2$ ceramic and lattice vibration, the infrared spectral data of the ceramic was analyzed based on classical harmonic oscillator model:

$$\varepsilon^*(\omega) = \varepsilon_\infty + \sum_{j=1}^{n} \frac{(z_j e)^2 / m_j V_j \varepsilon_0}{\omega_{Tj}^2 - \omega^2 - j\omega\gamma} \tag{11}$$

The z_j, m_j,V_j, γ_j, ω_{Tj}, and n in the above equation have been described at great length in the literature[42]. The association between permittivity and complex reflectance $R(\omega)$ can be represented as:

$$R(\omega) = \left| \frac{1 - \sqrt{\varepsilon^*(\omega)}}{1 + \sqrt{\varepsilon^*(\omega)}} \right|^2 \tag{12}$$

According to Equations (11) and (12), the infrared reflectance spectrum of $Y_{2.95}Dy_{0.05}MgAl_3SiO_{12}$-9wt%$TiO_2$ ceramic can be well fitted. In the microwave frequency region ($\omega << \omega_{Pj}$), the imaginary and real parts of complex permittivity ($\varepsilon^*(\omega)$) can be expressed as Equations (13) and (14) [43].

$$\varepsilon''(\omega) = \omega \sum_{j=1}^{n} \frac{\partial \varepsilon_j \gamma_j}{\omega_{Tj}^2} \tag{13}$$

$$\varepsilon'(\omega) = \varepsilon(\infty) + \sum_{j=1}^{n} \frac{\omega_{Pj}^2}{\omega_{Tj}^2} = \varepsilon(\infty) + \sum_{j=1}^{n} \partial \varepsilon_j \tag{14}$$

As shown in Fig. 5(a), the infrared reflectance spectrum can be well fitted with twelve Lorentzian modes, and the results are shown in Table 1. And the theoretical ε_r (~12.71) at 9.53 GHz is close to the measured value (~12.02). The calculated $Q \times f$ value of 33,321 GHz (f = 9.53 GHz, Q = 1/tan δ, tan δ = 2.86 × 10^{-4}) exceeds the measured value (28,604 GHz). The difference between measured and calculated values owing to the contribution of secondary phase, grain boundary and grain size to $Q \times f$ value.

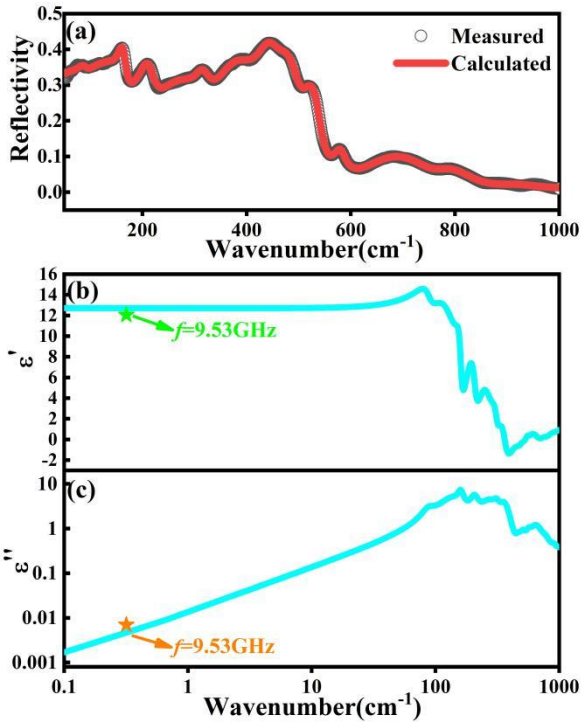

Fig. 5. (a) Fitted and experimental infrared reflection spectrum and (b-c) fitted complex dielectric spectrum of $Y_{2.95}Dy_{0.05}MgAl_3SiO_{12}$-9wt%$TiO_2$ ceramic.

Table 1

Phonon parameters obtained from the fitting of the infrared reflectivity spectra of $Y_{2.95}Dy_{0.05}MgAl_3SiO_{12}$-9wt%$TiO_2$ ceramic.

Mode	ω_{pj}	ω_{oj}	γ_j	$\triangle\varepsilon_j$	$\tan\delta_j\times10^{-4}$
1	31.823	90.865	12.864	0.123	0.142
2	133.58	163.45	15.808	0.668	0.0967
3	190.1	213.17	29.494	0.795	0.138
4	357.66	279.55	102.93	1.64	0.368
5	196.58	317.29	35.596	0.384	0.112
6	400.31	431.15	64.337	0.862	0.149
7	182.2	472.57	51.073	0.149	0.108
8	147	514.56	34.747	0.0816	0.0675
9	112.39	575.51	29.599	0.0381	0.0514
10	438.37	684.41	162.03	0.41	0.237
11	220.39	796.23	99.892	0.0766	0.125
12	255.29	931.76	173.61	0.0751	0.186

Dielectric resonators are one of the most important applications of microwave dielectric ceramics [44-46]. Following the publication of dielectric resonator antennas by Long et al. [47-48], the design of dielectric resonators as radiating antennas has gradually gained wide attention. For illustrating the possible application and goodness of temperature stable $Y_{2.95}Dy_{0.05}MgAl_3SiO_{12}$-9wt%$TiO_2$ ceramic, a temperature-stable 5G millimeter-wave dielectric resonator antenna was fabricated.

Fig. 6(a) and (b) depict the 3D structure diagram of the designed antenna. The antenna is fed using aperture coupling, with a rectangular dielectric resonator positioned directly above the aperture. The microstrip line is located at the bottom of the FR4 substrate, where two circular holes (r = 1.05 mm) facilitate the installation of SMA connector. The sizes of the DR, FR4 substrate and slot are $a\times a\times h$, $x\times x\times h_0$ and $l_s \times w_s$ (unit: mm), respectively. l_m is the stub extension and w_f denotes the width of the microstrip line. The specific parameter values are listed in Table 2. Fig. 6(c) and (d) are the upper surface and the lower surface of actual antenna, respectively. Fig. 6(e) shows that the measured and simulated S_{11} show good consistency. The center frequencies of measurement at 25 ℃ and 85 ℃ are 25.99 GHz and 26.12 GHz, respectively. The results prove the frequency shift is quite low, about 0.5%, showing a stable temperature property of the ceramic antenna. The bandwidth (S_{11} < -10dB) of measurement at 25℃ and 85 ℃ are 1.190 GHz and 1.140 GHz, respectively, which reflect the broadband characteristic of dielectric resonator antenna. Fig. 6 (f) shows the simulated impedance at 26.10 GHz. The impedance value of (50.29+1.14j) Ω is very close to 50 Ω, indicating that impedance matching is excellent, which can also be confirmed by the values of S_{11} in Fig. 6(e) are less than -30 dB. The simulated efficiency and gain in Fig. 6(g) are 88.5% and 6.05 dBi, respectively. Fig. 6(h) and (i) show the patterns of the cross-polarization and co-polarization of the E-plane and H-plane. In the boresight direction (θ=0°), the co-polarization field is over 20 dB stronger than cross-polarization field. Fig. 6 (j) and (k) are the three dimensional far-field radiation patterns at 26.10 GHz, which exhibit favorable radiation characteristics. According to the above results, the temperature-stable $Y_{2.95}Dy_{0.05}MgAl_3SiO_{12}$-9wt%$TiO_2$ ceramic antenna has a high potential application in 5G millimeter wave band.

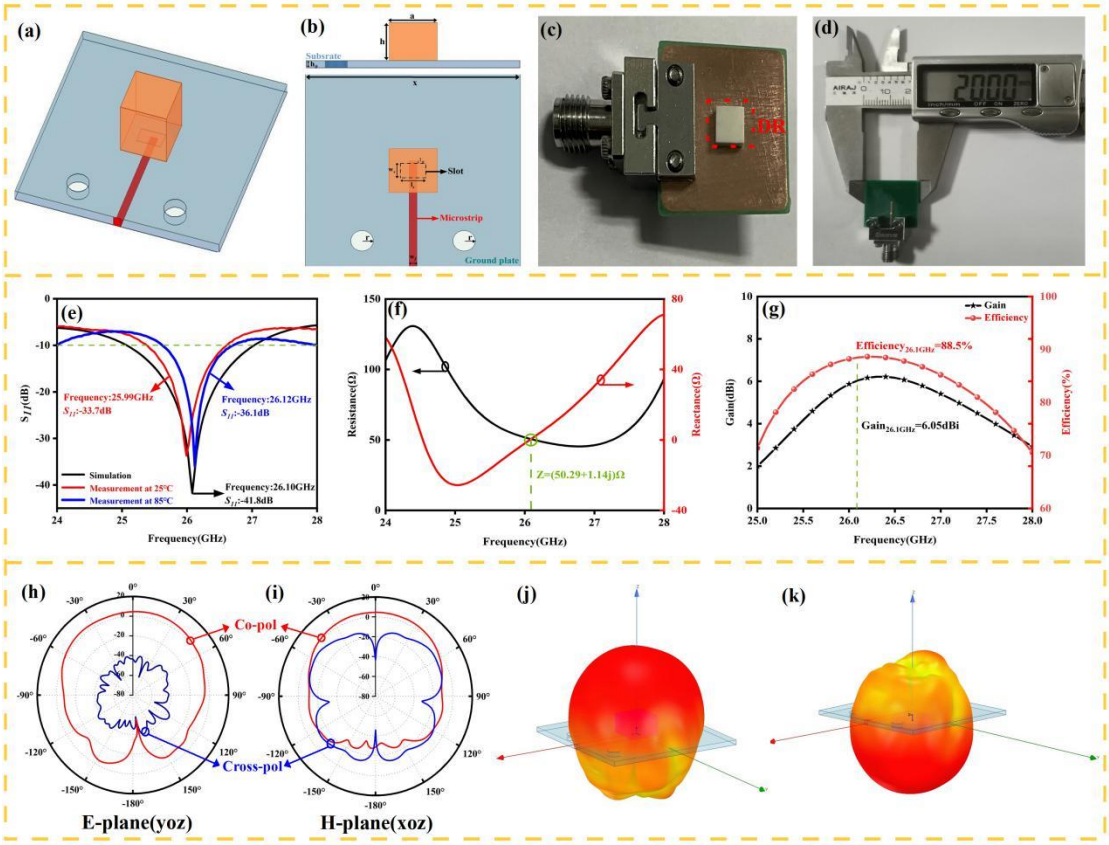

Fig. 6. (a) 3D structure drawing and (b) specific dimensions of the proposed antenna. (c) The upper surface and (d) the lower surface of actual antenna. (e) Simulated and measured return loss (S_{11}) at 25 ℃ and 85 ℃. (f) Simulated impedance of antenna. (g) Simulated efficiency and gain with various frequency. Cross-polarized and co-polarized of simulated (h) E-plane and (i) H-plane, (j) top and (k) bottom of simulated 3D radiation pattern at 26.10 GHz.

Table 2

The optimum parameters of the dielectric resonator antenna.

Parameters	a	h	x	h_0	l_s	w_s	l_m	w_f	r
Values(mm)	4.3	2.4	20	0.6	2.1	1.6	0.2	0.6	1.05

4. Conclusions

In this work, various mass percentages of TiO_2 were added to form composite ceramics to regulate the temperature coefficient of the $Y_{2.95}Dy_{0.05}MgAl_3SiO_{12}$ ceramic. The XRD patterns revealed that the main crystalline phase remained $Y_3Al_5O_{12}$ after the

addition of TiO_2, while $Y_2Ti_2O_7$ and TiO_2 appeared as secondary phases. Increasing the amount of TiO_2 decreased the $Q \times f$ value while increasing the ε_r and τ_f. Temperature stable composite ceramics are achieved for x = 9 wt% with ε_r = 12.06, $Q \times f$ = 28,604 GHz (f = 9.53 GHz), τ_f = -3.4 ppm/°C. The 5G millimeter-wave dielectric resonator antenna was fabricated based on the $Y_{2.95}Dy_{0.05}MgAl_3SiO_{12}$- 9wt%$TiO_2$ ceramic and tested at 25 ℃ and 85 ℃. The center frequencies of measurement at 25 ℃ and 85 ℃ are 25.99 GHz and 26.15 GHz, respectively, with the quite lower frequency shift of about 0.6%. The results suggest that the dielectric resonator antenna fabricated by temperature-stable $Y_{2.95}Dy_{0.05}MgAl_3SiO_{12}$-9wt%$TiO_2$ceramic has excellent temperature stability in millimeter wave band.

Declaration of Competing Interest

The authors declare that they have no known competing financial interests or personal relationships that could have appeared to influence the work reported in this paper.

Acknowledgements

This work was supported by the Natural Science Foundation of China (Grant No.52161145401, 51672063).

References

[1] R. Rehman, J.A. Sheikh, Compact high gain 28GHz concentric circular director low-cost antenna for 5G millimeter-wave communication, Lect. Notes. Electr. Eng. 694 (2021) 109-121.

[2] T.S. Rappaport, S. Sun, R. Mayzus, H. Zhao, Y. Azar, K. Wang, G.N. Wong, J.K. Schulz, M. Samimi, F. Gutierrez, Millimeter wave mobile communications for 5G cellular: It will work, IEEE. Access. 1 (2013) 335-349.

[3] Z.Y. Pi, F. Khan, An Introduction to Millimeter-Wave Mobile Broadband Systems, IEEE Commun. Mag. 49 (2011) 101-107.

[4] H.V. Pallavi, A.P. J. Chandra, Paramesha, Microstrip patch antenna analysis for 5G millimeter-wave communication: a survey, Lect. Notes. Electr. Eng. 752 (2021) 169-186.

[5] M.F. Zhou, C.C. Hu, J.B. Yin, Y. Jiang, B. Liu, K.X. Song, Cold sintering optimized SrF_2 microwave dielectric ceramics for the development of dielectric resonator antenna at 5G millimeter-wave band, Ceram. Int. (2022).

[6] B. Liu, K. Sha, M.F. Zhou, K.X. Song, Y.H. Huang, C.C. Hu, Novel low-ε_r MGa_2O_4(M=Ca, Sr) microwave dielectric ceramics for 5G antenna applications at the Sub-6 GHz band, J. Eur. Cearm. Soc. 41 (2021) 5170-5175.

[7] S.K. Zhu, Z.C. Huang, W.C. Lou, K.X. Song, A. Khesro, F. Hussain, Z.Y. Tan, X.J. Luo, M.M. Mao, L.Y. Xue, P. Xu, B. Liu, H.X. Lin, D.W. Wang, 5G microstrip patch antenna and microwave dielectric properties of 4mol%LiF- MgO-*x*wt%$MTiO_3$ (M = Ca, Sr) composite ceramics, J. Mater. Sci. Mater. Electron. 32 (2021) 23880-23888.

[8] Z. Yu, L.X. Li, M.K. Du, Ultra-high Q and low dielectric constant lithium titanate-based ceramics with outstanding wide temperature stability for millimeter wave microstrip antenna, J. Alloys. Compd. 887 (2021) 161436.

[9] Y. Zhan, L.X. Li, M.K. Du. The simulation for a high-efficiency millimeter wave microstrip antenna by low dielectric loss and wide temperature stable lithium-based microwave dielectric ceramics for LTCC applications, Ceram. Int. 47 (2021) 27462-27468.

[10] G.F. Wu, M.T. Ma, A.H. Li, K.X. Song, A. Khesro, H.B. Bafrooei, E.T. Nassaj, S.J. Luo, F. Shi, S.K. Sun, D.W. Wang, Crystal structure and microwave dielectric properties of Mg^{2+}-Si^{4+} co-modified yttrium aluminum garnet ceramics, J. Mater. Sci. Mater. Electron. 33 (2022) 4712-4720.

[11] I.M. Reaney, D. Iddles, Microwave dielectric ceramics for resonators and filters in mobile phone networks, J. Am. Ceram. Soc. 89 (2006) 2063-2072.

[12] X.Q. Song, F.F. Zeng, J.Q. Yang, C.Z. Yin, J.M. Wu, Y.S. Shi, W.Z. Lu, W. Lei, Crystal structure and microwave dielectric properties of garnet-type $Ca_2YZr_{2-x}Ti_xAl_3O_{12}$ ceramics for dual-band bandpass filters, J. Eur. Ceram. Soc. 42 (2022) 4962-4968.

[13] F.F. Wu, D. Zhou, C. Du, S.K. Sun, L.X. Pang, B.B. Jin, Z.M. Qi, J. Varghese, Q. Li, X.Q. Zhang, Temperature stable $Sm(Nb_{1-x}V_x)O_4$ ($0.0 \leq x \leq 0.9$) microwave dielectric ceramics with ultra-low dielectric loss for dielectric resonator antenna applications, J. Mater. Chem. C. 9 (2021) 9962-9971.

[14] W.C. Lou, K.X. Song, F. Hussain, A. Khesro, J.W. Zhao, H.B. Bafrooei, T. Zhou, B. Liu, M.M. Mao, K.W. Xu, E.T. Nassaj, D. Zhou, S.J. Luo, S.K. Sun, H.X. Lin,

D.W. Wang, Microwave dielectric properties of $Mg_{1.8}R_{0.2}Al_4Si_5O_{18}$(R=Mg, Ca, Sr, Ba, Mn, Co, Ni, Cu, Zn) cordierite ceramics and their application for 5G microstrip patch antenna, J. Eur. Ceram. Soc. 42 (2022) 2254-2260.

[15] H.H. Guo, D. Zhou, C. Du, P.J. Wang, W.F. Liu, L.X. Pang, Q.P. Wang, J.Z. Su, C. Singh, S. Trukhanov, Temperature stable $Li_2Ti_{0.75}(Mg_{1/3}Nb_{2/3})_{0.25}O_3$-based microwave dielectric ceramics with low sintering temperature and ultra-low dielectric loss for dielectric resonator antenna applications, J. Mater. Chem. C. 8 (2020) 4690-4700.

[16] J.F. Zurcher, On some thermal properties of microstrip antennas, Microwave. Opt. Technol. Lett. 10 (1995) 261-263.

[17] G. Drossos, Z. Wu, D. Lacey, L.E. Davis, Experimental investigation of a cylindrical dielectric resonator antenna at 77K, Microwave. Opt. Technol. Lett. 14 (1997) 62-64.

[18] M.X. Liu, J. Li, Y. Tang, J.Q. Chen, L.Y. Ao, A.L. Cao, L. Fang, Tunability of τ_f in garnet-structured $Y_3Ga_5O_{12}$ microwave dielectric ceramics, J. Eur. Ceram. Soc. 41 (2021) 7711-7716.

[19] M. Rakhi, G. Subodh, Crystal structure and microwave dielectric properties of $NaPb_2B_2V_3O_{12}$(B=Mg, Zn) ceramics, J. Eur. Ceram. Soc. 38 (2018) 4962-4966.

[20] Y. Tang, H. Li, J. Li, H.C. Xiang, L. Fang, Microwave dielectric properties of $Li_3A_3Te_2O_{12}$(A=Y, Yb) garnets for low temperature cofired ceramic technologies, J. Eur. Ceram. Soc. 42 (2022) 2248-2253.

[21] J. Li, Y. Tang, Z.W. Zhang, W.S. Fang, L.Y. Ao, A.H. Yang, L.J. Liu, L. Fang, Two novel garnet $Sr_3B_2Ge_3O_{12}$(B=Yb, Ho) microwave dielectric ceramics with low permittivity and high Q, J. Eur. Ceram. Soc. 42 (2021) 1317-1323.

[22] J.Q. Chen, Y. Tang, H.C. Xiang, L. Fang, H. Porwal, C.C. Li, Microwave dielectric properties and infared reflectivity spectra analysis of two novel low-firing $AgCa_2B_2V_3O_{12}$(B=Mg, Zn) ceramics with garnet structure, J. Eur. Ceram. Soc. 38 (2018) 4670-4676.

[23] Y. Tang, H. Li, J. Li, W.S. Fang, Y. Yang, Z.Y. Zhang, L. Fang, Relationship between Rattling Mg^{2+} ions and anomalous microwave dielectric behavior in $Ca_{3-x}Mg_{1+x}LiV_3O_{12}$ ceramics with garnet structure, J. Eur. Ceram. Soc. 41 (2021) 7697-7702.

[24] Y. Jiang, H. Liu, R. Muhammad, X.J. Luo, K.X. Song, M.M. Mao, S.K. Sun, H.B. Bafrooei, E.T. Nassaj, Y. Iqbal, R. Sun, D.W. Wang, Broadband and high-

efficiency of garnet-typed ceramic dielectric resonator antenna for 5G/6G communication application, Ceram.Int. (2022)

[25] C. Du, M.S. Fu, D. Zhou, H.H. Guo, H.T. Chen, J. Zhang, J.P. Wang, S.F. Wang, H.W. Liu, W.F. Liu, L. Li, Z. Xu, Dielectric resonator antenna with $Y_3Al_5O_{12}$ transparent dielectric ceramics for 5G millimeter-wave applications, J. Am.Ceram. Soc. 104 (2021) 4659-4668.

[26] L.Z. Ni, L.X. Li, M.K. Du, Y. Zhan, Wide temperature stable $Ba(Mg_xTa_{2/3})O_3$ microwave dielectric ceramics with ultra-high-Q applied for 5G dielectric filter, Ceram. Int. 47 (2021) 1034-1039.

[27] W. Jiang, X.W. Cheng, Z.P. Xiong, Z.L. Ma, T. Ali, H.N. Cai, J. Zhang, Static and dynamic mechanical properties of Yttrium Aluminum Garnet (YAG), Ceram. Int. 45 (2019) 12256-12263.

[28] M.K. Zhou, H.T. Chen, X. Zhang, B. Tang, Phase composition, microstructure, and microwave dielectric properties of non-stochiometric yttrium aluminum garnet ceramics, J. Eur. Ceram. Soc. 42 (2022) 472-477.

[29] J.B. Song, K.X. Song, J.S. Wei, H.X. Lin, J. Wu, J.M. Xu, W.T. Su, Z.Q. Cheng, Ionic occupation, structures, and microwave dielectric properties of $Y_3MgAl_3SiO_{12}$ garnet-type ceramics, J. Am. Ceram. Soc. 101 (2018) 244-151.

[30] Z.Y. Ma, W.J. Guo, Z.X. Yue, Microwave dielectric properties of Al-doped $Ba_4(Sm, Nd)_{9.33}Ti_{18}O_{54}$ ceramics added with TiO_2 and sintered in oxygen, Ceram. Int. 48 (2022) 12906-12913.

[31] A. Manan, R. Ullah, Y. Iqbal, A.S. Ahmad, A. Ullah, A.H. Wazir, Z.H. Yao, Tailoring the microwave dielectric properties of $Sr_{0.6}Ca_{0.4}LaAlO_4$ ceramic by TiO_2 addition, J. Aust. Ceram. Soc. 56 (2020) 1013-1019.

[32] A.A. Kishk, Dielectric resonator antenna, a candidate for radar applications, IEEE. Nat. Radar. Conf. Proc. (2003) 258-264.

[33] A. Petosa, Dielectric resonator antenna handbook, United States, 2007.

[34] K.M. Luk, K.W. Leung, Dielectric resonator antennas, England, 2002.

[35] H.R. Zheng, S.H. Yu, L.X. Li, X.S. Lyu, Z. Sun, S.L. Chen, Crystal structure, mixture behavior, and microwave dielectric properties of novel temperature stable $(1-x)MgMoO_4$-$xTiO_2$ composite ceramics, J. Eur. Ceram. Soc. 37 (2017) 4661-4665.

[36] Y.Y. Zhou, Z.X. Yue, L.T. Li, Preparation and microwave dielectric properties of TiO_2-doped YAG ceramics, Ferroelectrics. 407 (2010) 69-74.

[37] Z.Y. Tan, K.X. Song, H.B. Bafrooei, B. Liu, J. Wu, J.M. Xu, H.X. Lin, D.W. Wang, The effects of TiO_2 addition on microwave dielectric properties of $Y_3MgAl_3SiO_{12}$ ceramic for 5G application, Ceram. Int. 46 (2020) 15665-15669.

[38] X.J. Wang, J.J. Xie, Z.J. Wang, G.H. Zhou, Y. Shi, S.W. Wang, X.J. Mao, Fabrication and properties of $Y_2Ti_2O_7$ transparent ceramics with excess Y content, Ceram. Int. 44 (2018) 9514-9518.

[39] X.S. Lyu, L.X. Li, S. Zhang, H. Sun, B.W. Zhang, J.T. Li, M.K. Du, Crystal structure and microwave dielectric properties of novel (1-*x*)$ZnZrNb_2O_8$-*x*TiO_2 ceramics, Mater. Lett. 171 (2016) 129-132.

[40] J. Guo, D. Zhou, H. Wang, Y.H. Chen, Y. Zeng, F. Xiang, Y. Wu, X. Yao, Microwave and infrared dielectric response of temperature stable (1-*x*)$BaMoO_4$-*x*TiO_2 composite ceramics, J. Am. Ceram. Soc. 95 (2012) 232-237.

[41] H.D. Gu, C. Feng, H.O. Zhu, H.K. Zhu, X.F. Ding, L.X. Wang, G.H. Zhou, M. Wang, S.W. Ta, Q.T. Zhang, Effect of Li nonstoichiometry and TiO_2 addition on the microwave dielectric properties of Li_3PO_4 ceramics, Ceram.Int. 48 (2022) 20332-20340.

[42] H.H. Guo, D. Zhou, L.X. Pang, Z.M. Qi, Microwave dielectric properties of low firing temperature stable scheelite structured (Ca,Bi)(Mo,V)O_4 solid solution ceramics for LTCC applications, J. Eur. Ceram. Soc. 39 (2019) 2365-2373.

[43] C. Du, D. Zhou, L.P. Feng, T.T. Zhao, H.T. Chen, H.W. Liu, M.A. Darwish, S. Xia, Z. Xu, Wideband low-profile H-shaped dielectric patch antennas based microwave dielectric ceramics, Appl. Phys. Lett. 120 (2022) 223301.

[44] P. Tripathi, B. Sahu, S.P. Singh, O. Parkash, D. Kumar, Preparation and characterization of liquid phase ($55B_2O_3$-$45B_2O_3$) sintered cobalt doped magnesium titanate for wideband stacked rectangular dielectric resonator antenna(RDRA), Ceram. Int. 41 (2015) 2908-2916.

[45] P. Tripathi, P. Kumari, B. Sahu, R. Singh, S.P. Singh, D. Kumar, Filleted RDRA using novel ceramic dielectric (3G-BST) with stable gain and improved bandwidth for X-band application, Ceram. Int. 44 (2018) 5045-5054.

[46] L.O. Azevedo, S.J.T. Vasconcelos, H.D. Andrade, I.S.Q. Junior, R.S. Silva, A.S.B. Sombra, Design and characterization study of $LaFeO_3$ and $CaTiO_3$ composites at

microwave frequencies and their applications an dielectric resonator antennas, Ceram. Int. 47 (2021) 33232-33241.

[47] M.W. McAllister, S.A. Long, Resonant hemispherical dielectric antenna, Electron. Lett. 20 (1984) 657-659.

[48] M.W. McAllister, S.A. Long, G.L. Conway, Rectangular dielectric resonator antenna, Electron. Lett. 19 (1983) 218-219.